

Article

# The Limits of X-ray Diffraction Theory

Paul F. Fewster

Independent Researcher, Brighton BN1 9SB, UK; paul.f.fewster@gmail.com

**Abstract:** X-ray diffraction theory allows the interpretation of experiments to build a structural model that fits the collected data. As with any experimental science, the observations are subject to uncertainty through the instrument and user limitations. Similarly, the theory can never be perfectly complete; it will have limits, and therefore the resultant model will have uncertainties associated with it. This article discusses the limits of X-ray kinematical and dynamical diffraction theories. These are not the only theories, but are the most widely used. These theories are often extended to accommodate new findings, which can reach the stage at which their fundamental premise is clouded. At that point, the theory requires a rethink. There should be nothing sacrosanct about a theory; it should represent the best usable explanation that will allow a good interpretation of the data. Both kinematical and dynamical theories assume that the X-rays see an average structure, which is not what a photon experiences. The observed diffraction pattern is the average of the diffraction patterns created by all the photons, which is not the same as the diffraction pattern from the average structure. Accounting for this has a profound influence on the interpretation of the data.

**Keywords:** X-ray diffraction; theory; thermal vibrations; Ewald sphere; diffraction streaking

## 1. Introduction

All X-ray diffraction theories have limits, and knowing these is crucial to interpreting the data correctly [1]. Typically, conventional kinematical theory starts with Bragg's law and assumes a perfect crystal [2]. The profile shape is interpreted by including smearing functions, e.g., those due to crystal size broadening and diffuse scattering from defects. Ideally, a theory would include all known information about the X-ray photons and the full nature of the crystal under investigation. This is presently impractical since this requires intensive calculations. There is also the influence of the diffractometer to consider. The conventional kinematical theory is used in powder diffraction and single crystal structure determination, whereas the closest example of the more complete approach is used in the study of near perfect semiconductor crystals with dynamical theory. The reason for this is that the sample is very well defined and dynamical theory is a more exact description of the diffraction process. If, for example, Bragg's law and kinematical theory were applied to semiconductor heterostructures, the derived information will contain large errors [3], which are resolved by applying dynamical theory. However, when dynamical theory is applied to imperfect crystals it fails, although numerous authors have extended it to account for imperfections [4–7], etc. However, as will be illustrated, dynamical theory within this conventional formulation has its limits and cannot reproduce the whole of the diffraction pattern observed, even with perfect crystals.

The intensity calculated with the simpler kinematical theory and the dynamical theory are very different, unless the crystals are very small, i.e.,  $<1 \mu\text{m}$ . This is a result of extinction, where the diffracted beam is diffracted back into the path of the incident beam, reducing the diffracted intensity and the forward incident intensity. Dynamical theory includes this effect, and kinematical theory requires a subsequent correction. Therefore, understanding the nature of the crystal is important when judging which theory to use.

Suppose we have a perfect crystal, a perfect instrument and apply conventional two-beam dynamical theory (one incident beam and one diffracted beam [8]) but use it over a



**Citation:** Fewster, P.F. The Limits of X-ray Diffraction Theory. *Crystals* **2023**, *13*, 521. <https://doi.org/10.3390/cryst13030521>

Academic Editor: Borislav Angelov

Received: 27 February 2023

Revised: 11 March 2023

Accepted: 15 March 2023

Published: 18 March 2023



**Copyright:** © 2023 by the author. Licensee MDPI, Basel, Switzerland. This article is an open access article distributed under the terms and conditions of the Creative Commons Attribution (CC BY) license (<https://creativecommons.org/licenses/by/4.0/>).

large angular range or in extreme geometries, e.g., when the incident or diffracted beam is close to the surface, then the theory will fail to reproduce the experimental profiles [1]. This is because the diffraction from one reflection can interfere with another. By introducing a specular beam (surface reflection), the diffraction profile is more complete; see Figure 1 (effectively including all four tie points (intersections) of the dispersion surface in the two-beam theory). This improvement alone is still insufficient to produce the correct profile along the  $\langle 001 \rangle$  line of reflections from planes parallel to the surface. The two-beam dynamical theory only generates one reflection and requires as many beams as there are reflections to account for all the interferences in this profile. Introducing more reflections requires three-beam, four-beam, five-beam, etc., dynamical theory. These calculations become completely unwieldy [9] because they require the solution of  $n$  interacting dispersion surfaces to include  $n$ -beams. There is, though, an underlying problem in that, however generalized this dynamical theory becomes, it uses the structure factors for a discrete set of reciprocal lattice vectors. A kinematical theory can overcome this, but it cannot account for extinction and the peak intensities are incorrect. These examples indicate the limits of the conventional dynamical theory [5,6,8,10–12], etc. However, it is widely used and very useful within its limits, i.e., in the vicinity of one reflection. The two-beam (with two-tie points) dynamical theory is available commercially.

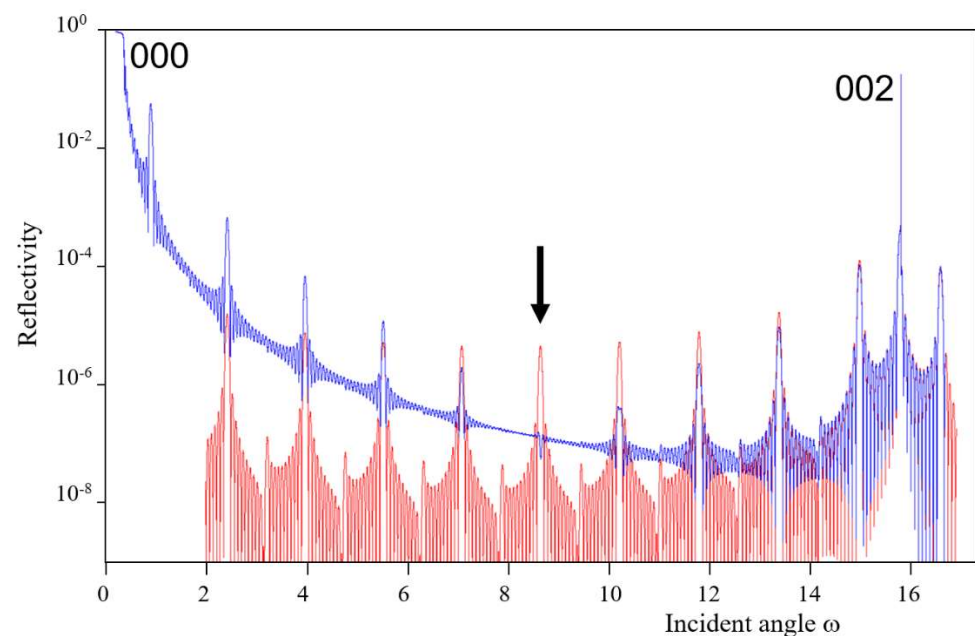


**Figure 1.** Two dynamical theory calculations; (red) the 2-beam theory calculations using 2-tie points of the dispersion surface for the 002 reflection and (blue) the 2-beam theory using 4-tie points for the 002 and 000 reflection on a superlattice sample  $\{\text{AlAs} (2.861 \text{ nm}) + \text{GaAs} (2.86 \text{ nm})\} \times 50$  on GaAs. The most used theory (red) deviates significantly beyond a few degrees from the 002 Bragg peak. This is especially notable at the arrow mark, where the superlattice peaks in the more complete theory are absent but present in the simpler theory. The incident angle  $\omega$  is the angle to the sample surface, which in this case is also the angle to the crystal planes  $\Omega$ .

## 2. An Alternative Dynamical Diffraction Description

Suppose the calculation is considered in a different way, by using the well-established Fresnel equations [13]. This approach generates all the transmitted and scattered waves and their interferences in a crystal, and is therefore fully dynamical. It removes Bragg's law and the dispersion surfaces and most of limitations of conventional dynamical theory [14]. The crystal is modelled as many very thin lamellae of constant scattering ability, which are parallel to the crystal planes (and in the most straightforward case, parallel to the surface). These lamellae have a thickness that is a small fraction of the repeat distance, or unit cell

(determined by trial and error), and the scattering ability is averaged laterally. This removes the discrete nature of the structure factor because the scattering factor is included as the profile of the electron distribution through the whole crystal.

The Fresnel formula was applied to each lamella, with the scattering from each being used as the input for the adjacent lamellae. The full diffraction profile is built by including all the lamellae throughout the crystal; see Figure 2. The whole diffraction profile is complete, including all diffraction orders. The calculation time takes longer than the commercially available two-beam dynamical diffraction calculations, but with optimisation it should be comparable, i.e., within seconds, depending on the complexity of the structure.

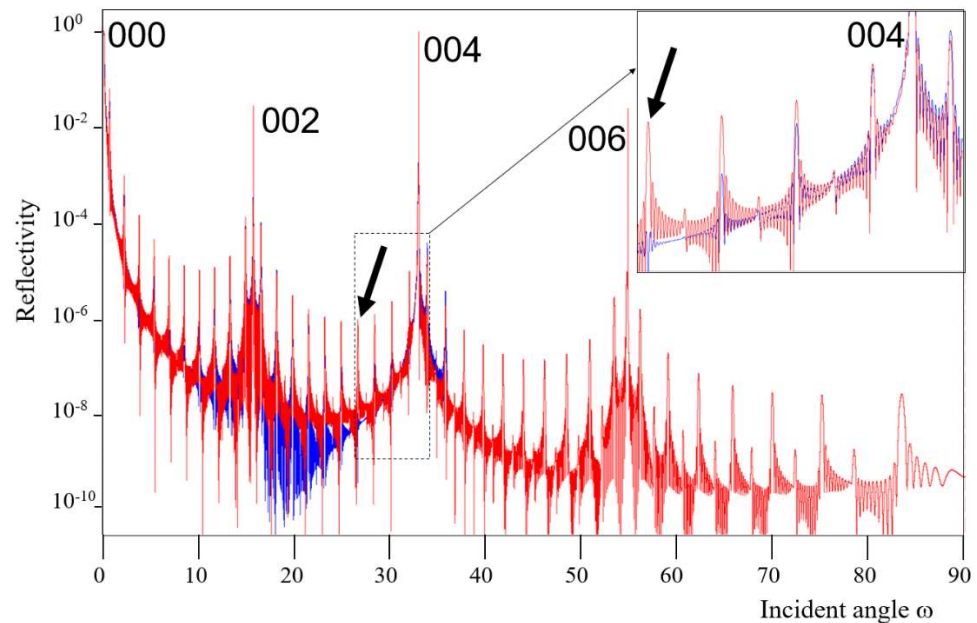


**Figure 2.** The simulation of the full diffraction profile (red) using the Fresnel theory compared with the 3-beam dynamical theory (000, 002 004 reflections, blue). The 3-beam dynamical theory simulation now includes the 004 peak (as well as the 000 and 002), and the profile has become closer to the more complete theory; however, there are still differences that are still clear around the 004 reflection (arrowed) because the 006 is not included.

This Fresnel approach has been applied to the *hhh* diffraction from a 111 surface orientated Si crystal [15]. The 222 diffraction peak appears and does not require any assumptions about asymmetric bonding, as suggested by Bragg [16]. The conventional (textbook) derivation of the structure factor would require the 222 intensity to be zero, which has led to a large field in determining the bonding asymmetry in crystals. This more complete theory based on the Fresnel formula suggests that these interpretations may be in error, unless a more complete theory is used as the base before interpreting deviations.

This Fresnel approach is computationally cumbersome, especially when deriving the scattering from inclined planes [14], but it has been used to predict some very subtle diffraction effects that have been observed experimentally [1], e.g., Aufhellung and Umweganregung [17]. It has also been used to simulate defects by modifying the average lateral scattering ability.

It appears, therefore, that this Fresnel dynamical diffraction theory is more complete for modelling perfect crystals compared with conventional dynamical theory. Despite this improvement, there are persistent diffraction features that are still not accommodated. These are revealed in experiments using very high resolution Reciprocal Space Mapping [18,19]. This mapping indicates intensity streaking close to the Bragg scattering angle  $2\theta_B$  over large crystal plane rotations away from the Bragg condition; see Figure 3a.

A  $2\theta$  profile scan reveals this as a peak (see Figure 3b and [20]), a feature that is easily overlooked. None of the theories above explain this streak or peak of intensity.

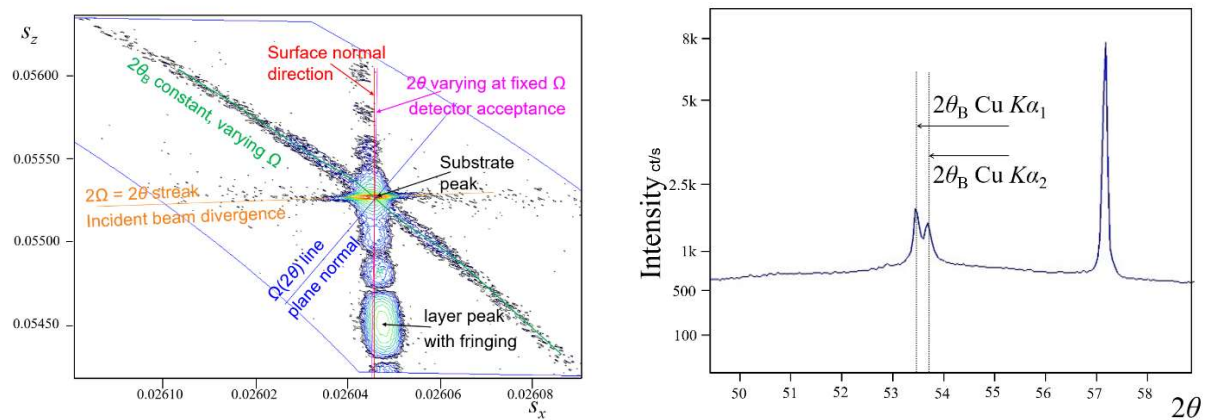


**Figure 3.** Experimental evidence of the streak of intensity close to  $2\theta_B$  with varying  $\Omega$ , observed from near perfect semiconductor crystals. (a) A reciprocal space map with a high-resolution diffraction configuration (single wavelength  $\text{Cu } K_{\alpha 1}$ , achieved with an X-ray mirror and grazing exit geometry, courtesy of J Woitok and A Karchenko) and (b) a  $2\theta$  scan with a fixed incident angle remote from the Bragg condition with both  $\text{Cu } K_{\alpha 1}$  and  $\text{Cu } K_{\alpha 2}$  present. In (b), there is a specular peak where  $2\theta = 2\Omega$ , and a peak where the scan crosses the streak at  $2\theta = 2\theta_B$ ; the former is single valued because all wavelengths reflect at the same angle, and the second peak scatters  $\text{Cu } K_{\alpha 1}$  and  $\text{Cu } K_{\alpha 2}$  wavelengths to their respective  $2\theta_B$  values. The 113 reflection from an InGaAs layer on a GaAs (001) wafer in (a) and a Ge (001) wafer crystal in (b).

### 3. Explaining the Diffraction Streak

The theories described above assume that the crystal is a perfect array or a time-averaged structure. The kinematical theory starts with point scatterers, dynamical theory with a polarizable scattering medium that responds to an electromagnetic wave, and the Fresnel approach assumes a laterally averaged refractive index over a small thickness. They all assume that the crystal is perfect or that diffraction comes from an average crystal configuration.

It is important to consider how a crystal appears to a photon travelling at the speed of light. Each atom ( $\sim 0.1$  nm) will be sampled in  $\sim 3 \times 10^{-19}$  s, but because all atoms vibrate with a much longer time-period (e.g.,  $\sim 10^{-13}$  s to  $\sim 10^{-14}$  s [21]) they will appear stationary to a photon and displaced from their averaged positions. Atom vibrations are unavoidable. The diffraction from a real crystal will, therefore, be the average diffraction pattern from all the photons, not the diffraction pattern from a crystal with the average atomic positions.

In conventional theories, the effects of thermal vibrations and defects are incorporated as a perturbation on the average perfect structure, which is clearly an inadequate approximation for vibrations that should be included before any calculation. This has consequences; for example, if an observed peak is labelled as a Bragg peak when it is not, because it arises from a streak, then the subsequent analysis will start to go astray (see Figure 3b).

The origin of this diffraction streak can be understood by reverting to a simple model. Take a hypothetical crystal with two planes, and only one atom on each plane A and P; see Figure 4. An incident beam, I, will be scattered radially from each point atom to form spherical waves [22]. The different path lengths along any given direction will result in phase differences and interference with a series of streaks of maximum intensity; see Figure 5a. The detector is assumed to be at a large distance compared to the atom separation, and the far-field or Fraunhofer diffraction theory is applicable [13]. The intensity is plotted with coordinates associated with the incident angle to the planes and the scattering angle (deviation from the incident beam direction). The important point to note is that the streak

of intensity stays close to  $2\theta_B$  over a large range of incident angles. The higher angle streak corresponds to the second diffraction order, where the path difference corresponds to two wavelengths,  $2\lambda$ .

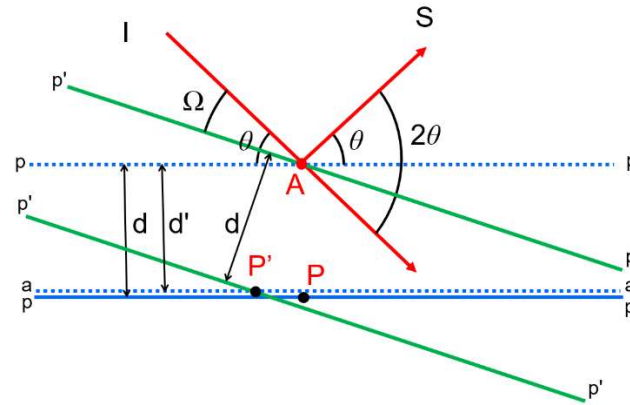


**Figure 4.** The atoms A and P sit on the planes pp and scatter radially. The scattering is at a maximum when the Bragg condition is satisfied, i.e., the distance between atoms on these parallel planes =  $\lambda/(2\sin\theta_B)$ . If the condition is satisfied when A and P scatter in phase  $d = \lambda/(2\sin\theta_B)$ , then any point along pp will be in-phase with A. When the crystal planes are rotated to  $p'p'$  the incident angle becomes  $\Omega$  and P rotates to the position  $P'$ . Following the argument above,  $P'$  now sits on a plane aa that is a distance  $d'$  from A. A and  $P'$  are in-phase when  $\theta = \sin^{-1}(\lambda/(2d'))$ , and for large movements in  $\Omega$  the change in  $d$  is very small, such that  $\theta$  barely changes.

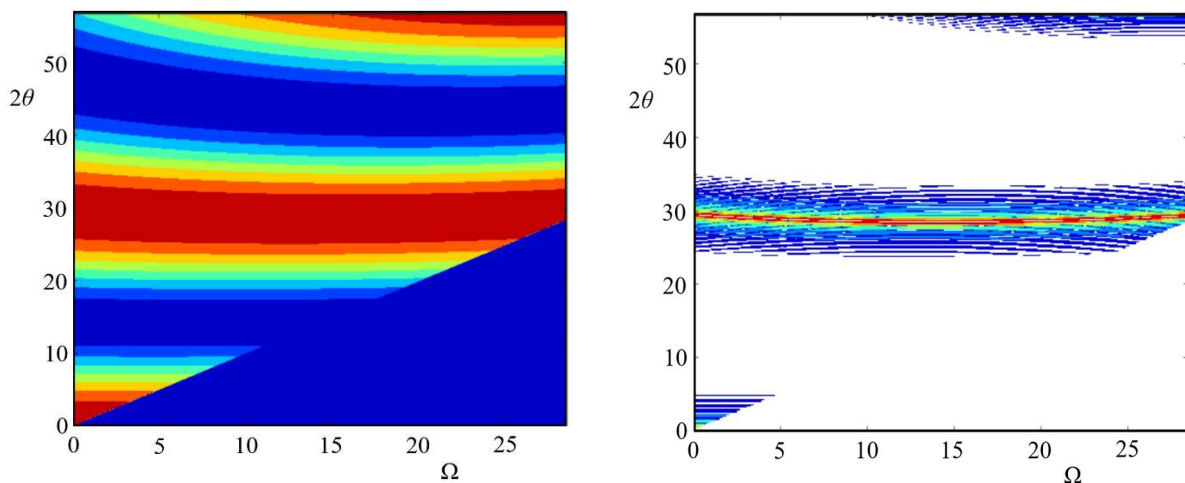


**Figure 5.** (a) The calculated scattering from two-point scatterers as the plane on which they sit is rotated (as in Figure 4). The intensity band at  $\sim 30^\circ$   $2\theta$  is close to the Bragg scattering angle, over the whole range of incident and scattering angles above the planes. (b) The same calculation with a column of 100-point scatterers.

By increasing the number of atoms to form a column (on many repeated planes), the streaks narrow; see Figure 5b. If more of these columns are combined by including more atoms on each plane, the streaking is suppressed. For infinite sized planes the streak disappears, which can be explained by the small shift in phase from column to column (due to the rotation) until one can be paired to the original that is exactly out of phase and their contributions cancel out. A finite size crystal will have interference features that correspond to the Fourier transform of the shape [23], which will not generally have streaks close to  $2\theta_B$ . However, this is the interpretation from a perfect array but not a real crystal. Any imperfections, unavoidable atom vibrations, etc., will weaken the phase cancellation, and the streaks, as in Figure 5, will begin to reappear.

The experimental evidence in Figure 3a can be explained by this description. Further support for this explanation comes from experiments using a multi-wavelength source, because the streak will simultaneously scatter for each wavelength at a fixed incident beam angle, as in Figure 3b [20]. Within the conventional description, only a single wavelength can be scattered at a single incident angle. This new theory indicates that a single incident beam will not only show peaks where a detector scan ( $2\theta$ ) intersects the expected shape interference pattern, but in addition will show a peak close to  $2\theta_B$  [15,20].

If the crystal is imperfect, e.g., if the crystal planes are not perfectly flat, then for a given incident beam direction there will be regions that satisfy the Bragg condition and scatter at  $2\theta_B$  and some that do not, but with scattered intensity close to  $2\theta_B$ . As the imperfections increase, a smaller proportion of the scattering can satisfy the Bragg condition at any given incident beam direction, which reduces the extinction effects in proportion and the diffracted intensity can be approximated by kinematical theory [15]. This is also compounded by the instrument used to collect the data.

A single crystal will have a diffraction width of the order of 5 to 10 s of arc (depending on various factors), and the beam divergence experienced by each point on a crystal plane will be typically 80 s of arc (i.e., assuming a slit-collimator, and a 200  $\mu\text{m}$  source at 0.5 m). This results in  $\sim 10\%$  of the incident beam within this divergence angle that satisfies the Bragg condition, and the remainder will be contributing to non-Bragg intensity of a varying magnitude. The Bragg condition will be stronger than non-Bragg intensities. This argument indicates that the ratio of non-Bragg to Bragg contributions is modified by the instrument.

Since the conventional description requires the observed peak intensity to come only from the Bragg condition, it must follow dynamical theory. For most crystals, kinematical theory applies and to explain this the crystals are assumed to be ideally imperfect and consists of mosaic blocks [8,24]. These blocks must be  $\sim <1 \mu\text{m}$  to follow kinematical theory. However, there is little evidence that the scattering from every crystal that follows kinematical theory has this specific microstructure. If, though, there are regions not in the Bragg condition due to local curvature from defects, there are still non-Bragg contributions that will contribute intensity towards  $2\theta_B$ . When this becomes a significant proportion of the scattering, the intensity will follow kinematical theory rather than dynamical theory. Point defects and dislocations are omnipresent in crystals, whereas mosaic blocks are not.

#### 4. Simulating the Diffraction Streak

Consider a crystal in more detail, or more specifically a crystal that an X-ray photon experiences. The parameters of a photon, including wavelength dispersion and length, are determined by its generation and, in the case of a laboratory source, the electron transition between energy levels in the target material. There is an uncertainty at the individual levels, and this gives an energy spread in the emitted photon  $\Delta E$ , which in turn gives the length of the photon  $\Delta x$  ( $\sim E\lambda/\Delta E$ ) and a wavelength spread  $\Delta\lambda$  [25]. The length of a photon gives rise to a 'coherence' length (the maximum path difference that a photon can interfere with itself, and it can only interfere with itself). Typically, for Cu  $K_{\alpha 1}$  radiation this coherence length is  $\sim 2 \mu\text{m}$ . This is significant when examining crystals larger than a few microns. As the scattering angle increases, the path difference between points of scatter decreases, and therefore the size of the regions that scatter coherently increases above the coherence length, i.e.,  $2\theta = 0$ , by  $1/\cos 2\theta$ . The diffractometer geometry can change the coherence length, e.g., non-dispersive geometry can reduce the overall path difference to give more overlap of the photon paths, which is comparable to increasing the coherence length.

It is clearly prohibitive to model the diffraction at a fundamental level because of the sheer complexity, but an indication can be obtained by representing atoms as point scatterers and a simple geometrical approach. Since the crystal must be small to have a manageable number of atoms even in this simple form, the influence of size effects can dominate ( $\sim 0.1 \mu\text{m}$  in this case, with  $1 \text{ nm}^3$  unit cells). To isolate the influence of the features of interest, the model structure was chosen to be an octagonal crystal with all the facets facing out of the scattering plane and stationary atoms. Each row of atoms was also varied

randomly by 5% to further reduce the dominance of the size effects. This gave a reference diffraction pattern from a crystal modelled in the conventional way; see Figure 6a. The diffraction pattern still has fringing normal to the facets (which fade more rapidly when they are out of the scattering plane).

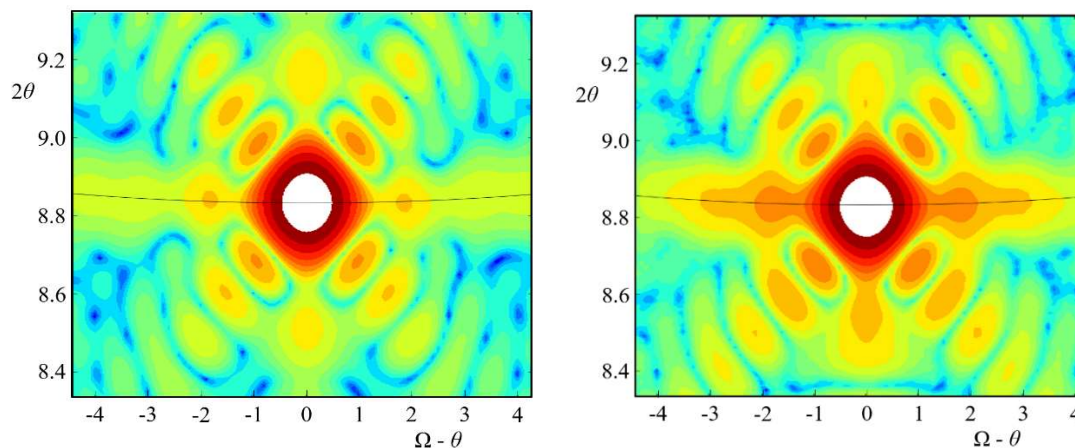


**Figure 6.** (a) The calculated diffraction pattern from an octahedron-shaped crystal (with its facets out of the plane of diffraction). This is the pattern for a perfect array of stationary point scatterers, with the dimensions on each row of atoms randomly varied by 5% to reduce the dominance of the shape effects. (b) The calculated diffraction pattern from a single photon interacting with the same crystal as in (a), but with each point scatterer having a positional uncertainty randomly sampled from a Gaussian distribution, with  $\sigma = 0.005$  nm to represent thermal vibrations and what a photon samples. The line of intensity enhancement close to the Bragg angle of  $8.82^\circ$  is clear to see in (b) compared with (a).

When atomic vibrations are included,  $\sim 0.005$  nm, the pattern changes significantly; see Figure 6b. These small random atom displacements produce an additional streak of intensity close to  $2\theta_B$ . In a real experiment, the diffraction pattern will be the sum of all the diffraction patterns from each photon used to collect the data. Calculated diffraction patterns from these atom vibrations all have the same broad characteristics.

## 5. The Impact of the Streaking on Kinematical Theory

### 5.1. Single Crystal Analyses

The presence of streaking described above from near perfect crystals is weak compared to the Bragg peaks. Most experiments on perfect crystals use high-resolution diffractometers, where the incident beam intensity is low compared to a powder diffractometer or an X-ray Free-electron Laser (XFEL) source. Since it is observed in the former, it should be a very noticeable feature in the latter two methods.

It is this underlying streaking close to  $2\theta_B$  that is the basis of the proposal in [26] to explain the data from powder diffraction experiments. The probability that a single crystal randomly orientated can satisfy the Bragg condition with a single wavelength source is negligible. This is a simple geometrical argument. The chance to observe several Bragg peaks simultaneously is, therefore, vanishingly small for typical X-ray wavelengths (for electron microscopy the wavelength is  $100\times$  smaller, making it less unlikely). Simultaneously measuring a few X-ray Bragg peaks has been a goal of those trying to solve the phase problem in crystallography, e.g., [27]. This method relies on very precise setups and careful measurements to observe multiple reflections. These are rare events.

However, six diffraction peaks are regularly observed from a single crystal snapshot with XFELs. If, as assumed, these peaks are solely due to Bragg scattering, then the geometrical explanation becomes complicated [28,29]. The high intensity of the source could easily reveal peaks close to their respective  $2\theta_B$ . In the powder diffraction case, the

large number of crystals will generate a vast number of scattering contributions close to  $2\theta_B$ , which will be additive.

During the testing of a very high intensity high-resolution diffractometer [30] based on “non-dispersive geometry”, a very weak  $\text{Cu } K_{\alpha 2}$  contribution was always present despite the incident beam on the analyser crystal being set for the  $\text{Cu } K_{\alpha 1}$  Bragg condition. The high intensity of this instrument gives a dynamic range of seven orders. It was not possible to eliminate a wavelength by selecting an incident beam direction, only by eliminating its scattered beam. This observation is explained by the new theory, i.e., any multi-wavelength beam incident on a crystal will scatter each wavelength close to its  $2\theta_B$ . This contribution was very weak because it was remote from the  $\text{Cu } K_{\alpha 2}$  Bragg condition for the reflection used. There are numerous features that can be explained by this theory [15]. Knowing the cause of this apparent artefact is helpful because it either limits the possibilities, or it can be accommodated in the analysis, modelled or can be an opportunity.

### 5.2. Powder Diffraction Analyses

This new theory explains many anomalies that occur in powder diffraction reliant on the conventional theory. It has been shown that the likelihood of the Bragg scattering occurring from typical numbers of randomly orientated crystals in a powder diffraction experiment is too low to account for the observations [26]. The diffractometer geometry used to collect each profile in Figure 7a would predict  $\sim 3$  Bragg condition peaks, which is exactly what is observed, but superimposed on top of a broad peak. The intensity was collected along  $2\theta$ , whilst keeping the incident angle fixed. There are a few sharp Bragg peaks, which have a width corresponding to the size of the crystallites, and the broad peak which can be explained by the dominance of the diffractometer geometry. This observation is in complete agreement with the predictions of the new theory; see Figure 7b. The peaks that appear from non-Bragg contributions have been exploited to create a small diffractometer for small samples [31]. The powder diffraction profile is, therefore, built from a distribution of intensities from Bragg and non-Bragg contributions associated with the crystal planes. The non-Bragg contributions contribute significantly to achieve reliable intensities. In the case of typical powder diffraction data, this distribution is close to completion because of the high number of contributions, and the intensities can be related directly to the structure factors [15].

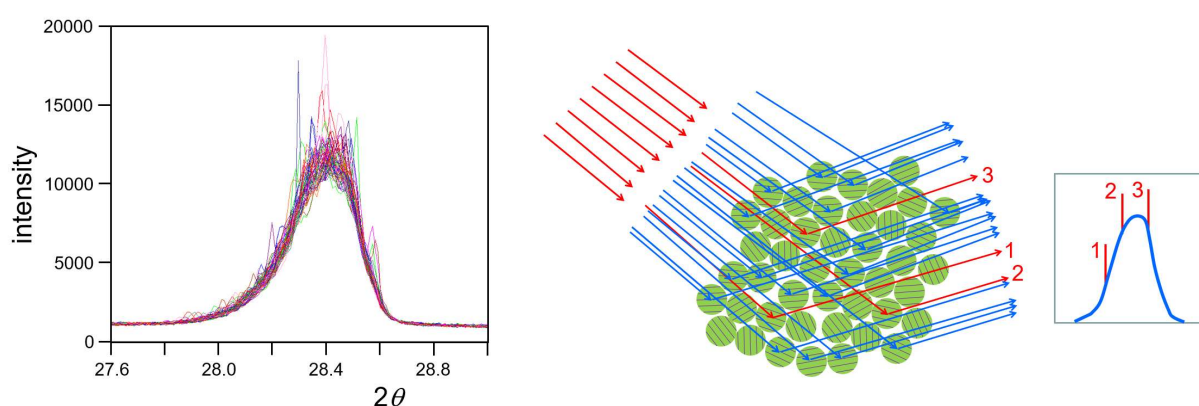


**Figure 7.** (a) A series of twenty superimposed profiles from a Si polycrystalline sample through a powder diffraction ring with a fixed incident angle (with a divergence of  $0.0625^\circ$  and  $2.3^\circ$  Soller slits) and a stationary position sensitive detector. The sample was rotated about an axis normal to the surface between each experiment. For each profile, there are two distinct regions, a few sharp peaks and a smooth broad profile. (b) A schematic of the origins of a profile. The divergent incident beam captures 3 crystals in the Bragg condition to form sharp peaks with widths corresponding to their size and a broad profile of non-Bragg contributions with a shape defined by the diffractometer geometry.

Another unresolved puzzle in powder diffraction has been the lattice parameter difference with single crystal studies. The former is smaller than the latter by about 20 ppm [32–34]. These were very carefully performed and precise measurements, which are very difficult to understand if all peaks are solely Bragg peaks. However, if the powder diffraction pattern includes contributions from the non-Bragg peaks, the lattice parameter is reduced by tens of ppm and accounts for this difference. This is because the contributions further from the Bragg condition shift to higher  $2\theta$  values, see Figure 6b, which creates a small bias towards lower lattice parameters when all the contributions are included.

### 5.3. The Ewald Sphere

The Ewald sphere is a widely used tool for X-ray crystallographers because it gives a clear indication when diffraction occurs. The dispersion surface construction in dynamical theory is a more exacting Ewald sphere construction that takes account of the polarizability of the electron wavefield distribution. The Ewald sphere and dispersion surface have radii of  $1/\text{wavelength}$  ( $1/\lambda$ ), and a crystal plane separation  $d$  will satisfy Bragg's law when the length vector  $1/d$  from the origin of reciprocal space touches the sphere surface; see Figure 8a. In dynamical theory, as more beams are added, more spheres of  $1/\lambda$  are included. These descriptions are built on each reciprocal lattice point for the 001, 002 and 003, reflections having lengths  $1/d_{001}$ ,  $1/d_{002}$  and  $1/d_{003}$ , which may contain atomic plane spacings that do not exist. Therefore, this cannot represent the diffraction process. From the Fresnel dynamical theory and the description of the new theory, Fewster (2014), the only length-scale in this sequence is  $1/d_{001}$ , i.e., the fundamental repeat distance, and the contributions associated with 002 and 003 are from path lengths of  $2\lambda$  and  $3\lambda$ , respectively. The Ewald sphere should be represented as a whole series of spheres of radii,  $1/\lambda$ ,  $1/2\lambda$ ,  $1/3\lambda$ , etc., to describe the diffraction process; see Figure 8b.

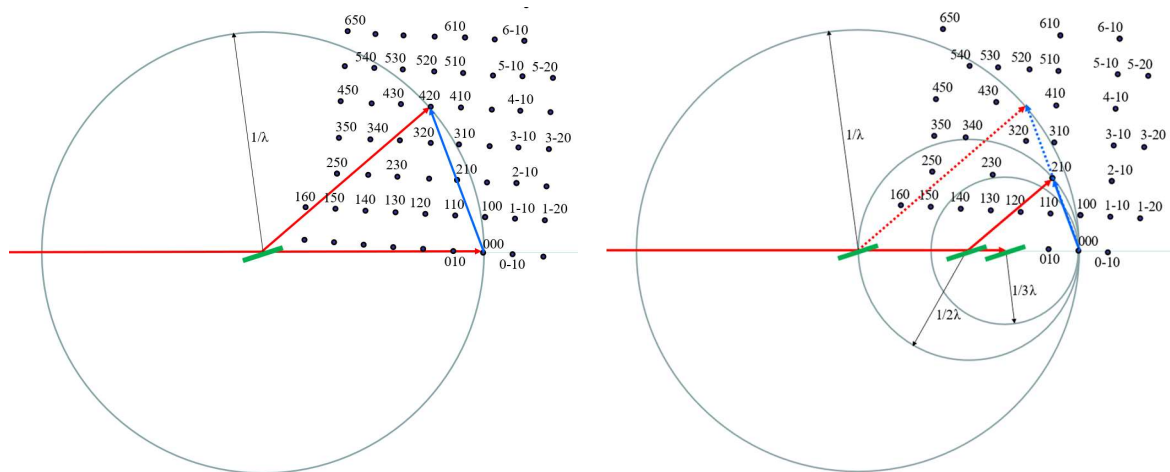


**Figure 8.** (a) Conventional Ewald sphere with a pathlength difference of one wavelength  $\lambda$ . (b) Ewald spheres based on pathlength differences of multiple wavelengths. The nested spheres in (b) only require the fundamental lengths to exist, e.g.,  $d_{210}$ , which avoids the situation in (a) where there may not be any atoms on planes separated by certain lengths, e.g.,  $d_{420}$ , making it confusing to visualise the diffraction process.

## 6. Concluding Remarks

The conventional kinematical and dynamical theories account for most features in a diffraction pattern. However, there are clear limits with dynamical theory away from the Bragg condition and questionable statistics associated with kinematical theory, e.g., the number and reliability of the peaks observed in powder diffraction, and the Bragg peaks in single crystal studies follow kinematical theory rather than dynamical theory, which is required at the Bragg condition.

There exists subtle streaking close to the Bragg scattering angle that is neither addressed nor can be accommodated in conventional theories and requires a physical explanation. This streak is always present, but weak, e.g.,  $\sim 10^{-3}$  to  $\sim 10^{-5}$  of the peak intensity in perfect crystals.

This streak can be explained by considering that each X-ray photon forms a diffraction snapshot of a crystal. The photon samples the atoms when they are distributed about their average positions through thermal vibrations. That is, the experimental observations are averages of the snapshots, NOT the average of the atom positions. Each snapshot no longer occurs from a perfect array, which in turn prevents the phase-cancellation of waves generated outside the Bragg condition. The effect is subtle, but profound.

The detector will intersect this streak and register weak peaks appearing close to the Bragg scattering angle, which can be remote from the Bragg condition. These peaks will be additive and create measurable intensity in powder diffraction scans. In an imperfect single crystal, the planes will not be perfectly flat and therefore the incident beam will scatter towards  $2\theta_B$  from regions that satisfy the Bragg condition and from regions not in the Bragg condition. Although the latter may be considerably weaker than the former, as the proportion of the non-Bragg diffraction increases compared to the Bragg condition diffraction, the intensity will change from dynamical to kinematical in nature.

**Funding:** This research received no external funding.

**Data Availability Statement:** The data is not available, the calculated data is from prototype software.

**Conflicts of Interest:** The author has no conflicts of interest.

## References

1. Fewster, P.F. *X-ray Scattering from Semiconductors and Other Materials*, 3rd ed.; World Scientific: Singapore, 2015; pp. 33–188.
2. Bragg, W.L. The Diffraction of Short Electromagnetic Waves by a Crystal. *Proc. Camb. Phil. Soc.* **1913**, *17*, 43–57.
3. Fewster, P.F.; Curling, C.J. Composition and lattice-mismatch measurement of thin semiconductor layers by X-ray diffraction. *J. Appl. Phys.* **1987**, *62*, 4154–4158. [[CrossRef](#)]
4. Penning, P.; Polder, D. Anomalous transmission of X-rays in elastically deformed crystals. *Philips Res. Rep.* **1961**, *16*, 419–440.
5. Takagi, S. Dynamical theory of diffraction applicable to crystals with any kind of small distortions. *Acta Cryst.* **1962**, *15*, 1311–1312. [[CrossRef](#)]
6. Takagi, S. A dynamical theory of diffraction for a distorted crystal. *J. Phys. Soc. Jpn.* **1969**, *26*, 1239–1253. [[CrossRef](#)]
7. Kato, N. Statistical dynamical theory of crystal diffraction. I. General formulation. *Acta Cryst.* **1980**, *A36*, 763–769. [[CrossRef](#)]
8. Authier, A. *Dynamical Theory of X-ray Diffraction*; Oxford University Press: New York, NY, USA, 2001.
9. Holý, V.; Fewster, P.F. Dynamical diffraction in layered systems—A quest for the final formula. *J. Phys. D Appl. Phys.* **2003**, *36*, A5–A8. [[CrossRef](#)]
10. Laue, M.V. Die dynamische Theorie der Röntgenstrahlinterferenzen in neuer Form. *Ergeb. Der Exakten Nat.* **1931**, *10*, 133–158.
11. Ewald, P.P. 1. Zur Begründung der Kristallographie. *Ann. Phys.* **1916**, *354*, 1–38. [[CrossRef](#)]
12. Ewald, P.P. 4. Zur Begründung der Kristallographie. *Ann. Phys.* **1917**, *359*, 519–556. [[CrossRef](#)]
13. Born, M.; Wolf, E. *Principles of Optics*, 4th ed.; Pergamon Press: Oxford, UK, 1970.
14. Holý, V.; Fewster, P.F. Crystal truncation rod X-ray scattering: Exact dynamical calculation. *J. Appl. Cryst.* **2008**, *41*, 18–26. [[CrossRef](#)]
15. Fewster, P.F. Estimating the structure factors in X-ray diffraction. *Acta Cryst.* **2018**, *A74*, 481–498. [[CrossRef](#)]
16. Bragg, W.H. The intensity of X-ray reflection by diamond. *Proc. Phys. Soc. Lond.* **1921**, *33*, 304–311. [[CrossRef](#)]
17. Renninger, M. ‘Umweganregung’, eine bisher unbeachtete Wechselwirkungserscheinung bei Raumgitterinterferenzen. *Z. Phys.* **1937**, *106*, 141–176. [[CrossRef](#)]
18. Fewster, P.F. A high-resolution multiple-crystal multiple-reflection diffractometer. *J. Appl. Cryst.* **1989**, *22*, 64–69. [[CrossRef](#)]
19. Fewster, P.F. Reciprocal Space Mapping. *Crit. Rev. Solid State Mater. Sci.* **1997**, *22*, 269–288. [[CrossRef](#)]
20. Fewster, P.F. What is an ‘ideally imperfect’ crystal? Is kinematical theory appropriate? *Acta Cryst.* **2016**, *A72*, 50–54.
21. Available online: [https://en.wikipedia.org/wiki/Molecular\\_vibration](https://en.wikipedia.org/wiki/Molecular_vibration) (accessed on 15 January 2023).
22. Huygens, C. *Traite de la Lumiere*; 1690; Chez Pierre van der Aa. Marchand Libraire: France. translated by Thompson, S.P. as *Treatise of Light*; Macmillan: London, UK, 1912.
23. Fraser, J.T.; Wark, J.S. Comments on a new theory of X-ray diffraction. *Acta Cryst.* **2018**, *A74*, 447–456. [[CrossRef](#)]
24. Darwin, C.G. The Reflection of X-rays from Imperfect Crystals. *Philos. Mag. Ser. 6* **1922**, *43*, 800–829. [[CrossRef](#)]
25. Heisenberg, W. Über den anschaulichen Inhalt der quantentheoretischen Kinematik und Mechanik. *Z. D Physik.* **1927**, *43*, 172–198. [[CrossRef](#)]

26. Fewster, P.F. A new theory for X-ray diffraction. *Acta Cryst.* **2014**, *A70*, 257–282. [[CrossRef](#)]
27. Chang, S.-L. *Multiple Diffraction of X-rays in Crystals*; Springer: New York, NY, USA, 1984.
28. White, T.A. Post-refinement method for snapshot serial crystallography. *Phil. Trans. R. Soc. B* **2014**, *369*, 20130330. [[CrossRef](#)] [[PubMed](#)]
29. Wojtas, D.H.; Ayyer, K.; Liang, M.; Mossou, E.; Romoli, F.; Seuring, C.; Beyerlein, K.R.; Bean, R.J.; Morgan, A.J.; Oberthuer, D.; et al. Analysis of XFEL serial diffraction data from individual crystalline fibrils. *IUCrJ* **2017**, *4*, 795–811. [[CrossRef](#)]
30. Fewster, P.F. A ‘beam-selection’ high-resolution X-ray diffractometer. *J. Appl. Cryst.* **2004**, *37*, 565–574. [[CrossRef](#)]
31. Fewster, P.F.; Trout, D.R.D. A compact high-resolution X-ray powder diffractometer. *J. Appl. Cryst.* **2013**, *46*, 1626–1639. [[CrossRef](#)] [[PubMed](#)]
32. Hart, M.; Parrish, W.; Bellotto, M.; Lim, G.S. The refractive-index correction in powder diffraction. *Acta Cryst.* **1988**, *A44*, 193–197. [[CrossRef](#)]
33. Hart, M.; Cernik, R.J.; Parrish, W.; Toraya, H. Lattice-parameter determination for powders using synchrotron radiation. *J. Appl. Cryst.* **1990**, *23*, 286–291. [[CrossRef](#)]
34. Becker, P.; Dorenwendt, K.; Ebeling, G.; Lauer, R.; Lucas, W.; Probst, R.; Rademacher, H.-J.; Reim, G.; Seyfried, P.; Siegert, H. Absolute Measurement of the (220) Lattice Plane Spacing in a Silicon Crystal. *Phys. Rev. Lett.* **1981**, *46*, 1540–1543. [[CrossRef](#)]

**Disclaimer/Publisher’s Note:** The statements, opinions and data contained in all publications are solely those of the individual author(s) and contributor(s) and not of MDPI and/or the editor(s). MDPI and/or the editor(s) disclaim responsibility for any injury to people or property resulting from any ideas, methods, instructions or products referred to in the content.